UDC 539. 4

Microstural Features of Failure Surfaces and Low-Temperature Mechanical Properties of Ti–6Al–4V ELI Ultra-Fine Grained Alloy

E. D. Tabachnikova,[1,a] A. V. Podolskiy,[1,b] V. Z. Bengus,[1,c] S. N. Smirnov,[1,d] K. Csach,[2,e] J. Miškuf,[2] L. R. Saitova,[3] I. P. Semenova,[3,f] and R. Z. Valiev[3,g]

[1] Verkin Institute for Low Temperature Physics & Engineering, National Academy of Sciences of Ukraine, Kharkov, Ukraine

[2] Institute of Experimental Physics, Academy of Sciences of Slovakia, Kosice, Slovakia

[3] Institute of Physics of Advanced Materials, USATU, Ufa, Russia

[a] tabachnikova@ilt.kharkov.ua, [b] podolskiy@ilt.kharkov.ua, [c] bengus@ilt.kharkov.ua, [d] smirnov@ilt.kharkov.ua, [e] csach@saske.sk, [f] semenova-ip@mail.ru, [g] rzvaliev@mail.rb.ru

Microstructural regularities of failure surfaces and low-temperature mechanical characteristics in quasistatic uniaxial tension and compression have been studied for ultra-fine grained structural states of Ti–6Al–4V ELI alloy processed by equal channel angular pressing. Values of the yield stress and uniform strain at 300, 77, and 4.2 K have been compared for structural states of the Ti–6Al–4V ELI alloy that differ in the average grain size and the morphology of α and β phases. Statistical distributions of dimple sizes on the failure surfaces have been studied for different structural states and temperatures.

Keywords: equal channel angular pressing, mechanical properties, low temperatures.

Experimental Materials and Procedures. The investigations have been carried out using Ti–6Al–4V ELI polycrystalline rods for medical applications (Intrinsic Devices Company, USA), and their composition was (wt.%): Ti = base, 6.0 Al; 4.2 V; 0.2 Fe; 0.001 C; 0.11 O; 0.0025 N; 0.002 H.

Mechanical characteristics have been studied in uniaxial tension and compression with a $4 \cdot 10^{-4}$ s^{-1} strain rate using a stiff straining machine at 300, 77, and 4.2 K. The specimens for tension had a 5.5 mm gauge length and a square cross section of 0.75×2.4 mm. Specimens for compression were rectangular prisms $2 \times 2 \times 7$ mm.

The yield stress $\sigma_{0.2}$, ultimate strength σ_u, uniform plastic strain ε_u (plastic strain prior to the neck formation in the case of tension), and the strain to failure ε_f have been measured from stress–strain curves.

The type of failure has been specified, and the failure surface morphology has been studied with a TESLA BS-300 scanning electron microscope (SEM).

Three structural states of the Ti–6Al–4V ELI alloy have been investigated:

State 1: initial polycrystalline alloy with approximately 12% of β phase, α grains have elongated shape with averaged sizes of 5–10 and 20–25 μm, respectively, β phase in the initial microstructure forms an interlayer between α grains.

State 2: billets 40 mm in diameter and 150 mm long were processed at 600°C by four ECAP passes with a 90° rotation around the billet axis in a die-set with a channel intersection angle of 120°. After the equal channel angular pressing (ECAP), the average grain size in the α phase is 0.5–1.0 μm. The quantity of the β phase decreases after the ECAP from 12 to 8%. Colonies of twins are a very important feature of this state. Their thickness is between 50 to 100 nm and the length is comparable with the average grain sizes (0.5 and 1.0 μm) [1].

State 3: thermal treatment of initial polycrystalline rods was carried out. Billets 40 mm in diameter and 150 mm long were heated up to 950°C, quenched in water, and further aged. Then, the billet was processed at 600°C by four ECAP passes, which was followed by

multi-cycle extrusion at 300°C. This has resulted in a highly dispersed structure (α phase fragments ranged from 200 to 400 nm) [1]. The volume fraction of the β phase was 5%.

Mechanical Characteristics of Ti–6Al–4V ELI Alloy. The averaged values of the yield stress $\sigma_{0.2}$, the ultimate strength σ_u, the uniform plastic strain ε_u, and the strain to failure ε_f for all structural states of the Ti–6Al–4V ELI alloy tested in tension and compression at 300, 77, and 4.2 K are listed in Table 1.

Table 1

Mechanical Characteristics of Ti–6Al–4V ELI Alloy in the Initial Coarse-Grained State 1 and Ultra-Fine Grained States 2 and 3 under Tension and Compression

Temperature (K)	Structural state	Tension				Compression		
		$\sigma_{0.2}$, GPa	σ_u, GPa	ε_u	ε_f	$\sigma_{0.2}$, GPa	σ_u, GPa	ε_f
300	State 1	0.80	0.91	0.10	0.17			
	State 2	0.98	1.03	0.04	0.07	1.10	1.28	0.13
	State 3	1.23	1.30	0.04	0.08			
77	State 1	0.99	1.08	0.15	0.19			
	State 2	1.49	1.57	0.03	0.06	1.58	1.63	0.02
	State 3	1.76	1.90	0.03	0.07			
4.2	State 1	1.59	1.66	0.06	0.06			
	State 2		1.69			1.84	2.14	0.06
	State 3		1.50					

The grain structure modification and the decrease in the grain sizes through the ECAP processing lead to a considerable increase in the alloy yield stress $\sigma_{0.2}$. In the ultra-fine grained state 2 the yield stress increases by 22.5% at 300 K and by 50% at 77 K as compared to the initial coarse-grained state 1. Heat treatment before the ECAP and the extrusion stimulate a further decrease of the grain size (state 3) and result in an additional increment of the yield stress $\sigma_{0.2}$ in comparison with state 2 (25.5% at 300 K and 18% at 77 K).

The difference in the $\sigma_{0.2}$ values in compression and tension (the so-called SD effect) is observed for state 2 and its value is 12% at 300 K and 6% at 77 K.

The change of the structural state from 1 to 2 has led to a decrease of the uniform plastic strain ε_u from 10 to 4% at 300 K, and from 15 to 3% at 77 K as it is shown in Table 1. In state 3, the uniform strain ε_u practically coincides with the value obtained for state 2 at 300 and 77 K.

At 4.2 K all specimens in states 2 and 3 fractured without macroscopic plastic deformation. Only failure stress values are listed in Table 1 for these cases.

Analysis of Failure Surfaces. Failure surfaces of specimens in states 1 and 2, which were tested under uniaxial tension at 300, 77, and 4.2 K, are oriented at an angle of 45° (shear failure), as well as 90° (normal failure) with respect to the tensile axis. In state 3, failure of specimens at 77 and 4.2 K took place only along different shear planes oriented at an angle of 45° to the tensile axis.

It is important to note that only ductile failure and typical dimple failure morphology were observed under uniaxial tension for all structural states of the specimens, which had been deformed at 300, 77, and 4.2 K. A typical morphology of the failure surfaces is shown in Fig. 1a and 1b. As one can see, the surfaces of shear failure have the dimple pattern that is elongated in the direction of the shear crack propagation (Fig. 1a), while the surfaces of "normal failure" have no elongation of the dimple pattern (Fig. 1b).

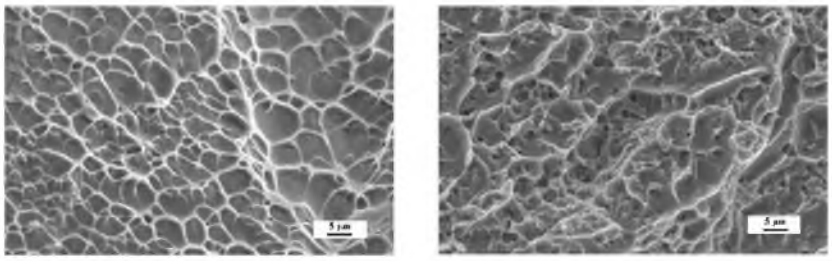

a b

Fig. 1. Failure surfaces of the Ti–6Al–4V ELI alloy subjected to tension at 77 K: (a) state 2: "shear failure"; (b) state 2: "normal failure"; SEM.

It is of interest to study the dependence of the dimple size on the structural state of the specimens as well as on the temperature of the experiment. Distributions of the dimple sizes on the failure surfaces have been obtained for the normal failure as well as for the shear failure at 300, 77, and 4.2 K for all three structural states studied. Examples of typical dimple size distributions for 77 K are shown in Fig. 2.

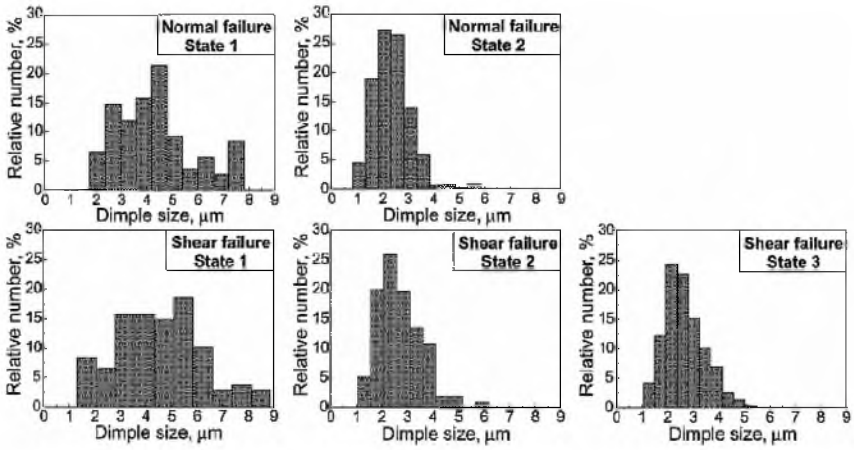

Fig. 2. Typical dimple size distributions as observed on the normal and shear failure surfaces of the Ti–6Al–4V ELI alloy after deformation at 77 K.

The distributions of the dimple sizes are not uniform for all cases studied. Table 2 contains average values of dimple sizes for all temperatures and structural states investigated.

Analysis of the obtained dimple size distributions can be summarized as follows:

(i) the obtained dimple size distributions have a small dependence on the experiment temperature;

(ii) transition from state 1 to states 2 and 3 leads to a decrease in the average dimple sizes;

(iii) dimple size distributions change their shape at transition from state 1 to states 2 and 3 and become more sharp;

(iv) the maximum of the dimple size distribution is considerably higher for states 2 and 3 in comparison with state 1.

It is noteworthy that the observed increase in the height of the dimple distribution maximum can be associated with differences in the distributions of structural inhomogeneities of these states. Thus, a wider distribution of grain sizes has been observed in structural state 1 (5–25 μm) as compared with states 2 (0.5–1.0 μm) and 3 (0.2–0.4 μm).

Table 2

Average Dimple Size Values for All Investigated Structural States of the Ti–6Al–4V ELI Alloy

Temperature (K)	Average dimple size					
	Normal failure			Shear failure		
	State 1 $d \sim 20$ μm	State 2 $d \sim 0.7$ μm	State 3 $d \sim 0.3$ μm	State 1 $d \sim 20$ μm	State 2 $d \sim 0.7$ μm	State 3 $d \sim 0.3$ μm
300	3.3	1.9	2.0	4.3	2.7	2.3
77	4.3	2.7		4.6	2.9	2.7
4.2	4.5	2.7		3.8	2.6	3.1

Discussion of Results. The observed increase in the yield stress $\sigma_{0.2}$ and decrease of the uniform strain ε_u in state 2 as compared with state 1 of the Ti–6Al–4V ELI alloy are explained by the presence of additional strong barriers for the dislocation slip in the form of grain boundaries and twin colonies in state 2. Further 20% increase in $\sigma_{0.2}$ in state 3, as compared with state 2, is apparently associated with a decrease in the average grain size that leads to an increase in the specific grain boundary area that represents an effective barrier for dislocations.

It is noteworthy that uniform strain values for states 2 and 3 practically coincide at 300 K, as well as at 77 K. Such behavior can be explained by a rather similar character of microstructures: colonies of twins in state 2 and boundaries of α grains in state 3 can be considered naturally as strong barriers for dislocation slip. Dislocation pile-ups that are formed in front of such barriers can stimulate microcrack nucleation. This may explain the presence of small plastic deformations in states 2 and 3 at 300 and 77 K.

Failure of specimens at 4.2 K in states 2 and 3 took place without macroscopic plastic deformation, but only ductile shear fracture was observed on the failure surfaces of those specimens. So, in this case, plastic deformation is localized and took place only in the region of the fracture crack.

The SD effect observed for ultra-fine grained state 2 of Ti–6Al–4V ELI alloy can be explained by the influence of pressure on the dislocation sources. And the difference in tension/compression local pressures increases with decreasing grain size [2].

It is known from the literature [3] that the typical dimple size on the failure surface of coarse-grained materials does not exceed the grain size, and the distribution of dimples on the failure surface frequently has a maximum, which corresponds to the typical size of the grain substructure [3]. Similar behavior is observed in the present work for state 1 (Fig. 2). But for ultra-fine grained states 2 and 3 the dimple size maximum exceeds considerably the grain sizes, and the grain boundary is not an effective barrier for dimple growth. Such effect was observed in nanocrystalline materials [4, 5], and it can be caused by the process of "clustering" (grouping of several adjacent grains during plastic deformation of nanocrystals) [4, 5]. And the size of such clusters in our case can be the characteristic structural size that corresponds to the dimple size distribution maximum.

1. I. P. Semenova., L. R. Saitova, G. I. Raab, et al., *Mater. Sci. Forum*, **503-504**, 757–762 (2006).
2. S. Cheng, J. A. Spencer, and W. W. Milligan, "Strength and tension/compression asymmetry in nanostructured and ultrafine-grain metals," *Acta Mater.*, **51**, 4505–4518 (2003).
3. V. I. Betekhtin and A. G. Kadomtsev, *Phys. Solid State*, **47**, 825–831 (2005).
4. A. Hasnaoui, H. Van Swygenhoven, and P. M. Derlet, *Science*, **300**, 1550 (2003).
5. H. Li, F. Ebrahimi, H. Choo, and P. K. Liaw, *J. Mater. Sci.*, **41**, 7636–7642 (2006).

Received 28. 06. 2007